





Guiding particles along arbitrary trajectories by circular Pearcey-like vortex beams

Danlin Xu , Zhenwu Mo, Junjie Jiang, Haoyu Huang , Quanfeng Wei, You Wu , Xinyue Wang, Zehong Liang, Haobin Yang, Hechong Chen, Haiqi Huang, Hongzhan Liu, Dongmei Deng,^{*} and Lingling Shui [†]
School of Information and Optoelectronic Science and Engineering, South China Normal University, Guangzhou 510006, China
and Provincial Key Laboratory of Nanophotonic Functional Materials and Devices, South China Normal University, Guangzhou 510631, China



(Received 3 March 2022; accepted 24 June 2022; published 13 July 2022)

A type of circular Pearcey-like vortex beam (CPLVB) is introduced numerically and experimentally, combining the properties of self-acceleration and abruptly autofocusing in the off-axis position. The interplay between the spiral phase and the modulated phase of arbitrary predesigned trajectories assists the beam to present a special shape which is suitable for manipulating and guiding particles along arbitrary trajectories. The beam propagating along the hyperbolic, hyperbolic secant trajectories generates a twisting hollow guide channel, and a parabolic bottle-like structure is constructed when the beam accelerates along the parabolic trajectory. Furthermore, the generation of the CPLVB, stable trapping, and rotation motion of micron-sized particles and transport of light-absorbing particles in air are realized in the experiment. Our results may bring about possibilities for wave front control, optical guidance, and manipulation of particles.

DOI: [10.1103/PhysRevA.106.013509](https://doi.org/10.1103/PhysRevA.106.013509)

I. INTRODUCTION

The abruptly autofocusing (AAF) fields which enable a low-intensity profile while suddenly releasing all their energy right before a target were firstly proposed theoretically [1] and verified experimentally [2]. Such intrinsic behavior results in the caustic with intensity maxima converging to the focus in a nonlinear fashion. Since then, different kinds of AAF beams have been reported [3–5] owing to their practical applications in medical laser treatments [1], particle manipulation [6], and multiphoton polymerization [7]. Among them, circular Pearcey beams have attracted considerable attention due to their peculiar properties including enhanced peak intensity contrast, shorter focal distances, and no oscillation after finishing the autofocus process [5]. By superimposing different phase structures to modulate the circular Pearcey beams, variant types of optical modes such as circular Pearcey beams with annular spiral-zone phase [8], and ring Pearcey beams with a cross phase [9] have also been introduced.

Optical vortex (OV) is characterized by carrying orbital angular momenta (OAM), exhibiting a helical wave front and hollow-core intensity distributions due to the existence of spatial phase singularity [10], which further boosts practical applications in optical communications [11], particle manipulation [12], and high-dimensional quantum cryptography [13]. Early researches about vortex beams concentrated on Laguerre-Gaussian modes [14]. With the development of OAM manipulation, vortex beams are demonstrated to form an optical spanner for controlled rotation of particles, expanding the applications of optical tweezers [15–17]. In recent years, OVs have been delivered with the diffraction-

free beams such as Mathieu and Bessel beams [18,19], and the vector modulation of vortex beams in linear and nonlinear media has been researched extensively [20,21]. Meanwhile, OVs are nested in different modes of structured light beams for extending plentiful applications; as a result, different phase profiles and intensity distributions can be obtained and some interesting phenomena are presented [22,23]. In particular, OVs intentionally delivered into self-accelerating Airy beams will follow curve paths of the main lobe, which introduces an innovative way in beam steering [24].

Airy beams endowed with self-acceleration, allowing the transport of particles along a parabola while bypassing obstacles, were initially proposed and observed by Siviloglou *et al.* [25,26]. Inspired by it, various approaches have been developed for generating spatially accelerating beams along arbitrary trajectories so as to improve the robustness for specific applications. The nondiffracting spatially accelerating beams following a circular trajectory are presented by solving the Maxwell equations [27]. The nonparaxial Mathieu and Weber beams propagating along elliptical and parabolic trajectories, respectively, are also obtained in experiment by solving the Helmholtz function [28]. Instead of finding analytical solutions of wave equations, the generation of arbitrarily accelerating beams is implemented by employing the approaches such as combined phase and amplitude modulation [29], spectral phase gradient [30], and phase superposition [31]. Moreover, through manufacturing the special materials including linear index potentials [32], nonlinear photorefractive crystals [33], and metamaterial [34], the beams can be controlled to move on arbitrary trajectories.

Ashkin's pioneering research about optical tweezers based on the radiation pressures [35] leads to a broad range of applications ranging from trapping of atoms [36], nanoparticles [37], microsized particles [38], and single molecules [39] to living cells [40]. The recent decade has seen significant progress in the use of structured light beams with customized

^{*}dengdongmei@m.scnu.edu.cn

[†]shuill@m.scnu.edu.cn

phase [41], amplitude [42], and controllable polarization [43] in optical trapping and rotation of particles by exerting optical forces arising from high intensity and phase gradients [44,45]. As for the light-absorbing particles, there exists another type of optical force named as photophoresis force being several orders of magnitude larger than the radiation forces [46], which can be tailored to realize controllable all-optical manipulation [47]. Therefore, many efforts have been put into demonstrating the possibility not only to stably trap but also to transport light-absorbing particles in air by the photophoretic force. Such particle manipulation can be achieved relying on the design and generation of optical bottle beams [48], the superposition and reshaping of optical vortex beams [49], and the use of cylindrical vector beams [50]. The question we address is whether we can deliver the OVVs with modulated optical beams following arbitrary curves, so as to form optical channels to guide particles along arbitrary trajectories.

In this paper, a type of circular Pearcey-like vortex beam (CPLVB) is introduced numerically and realized experimentally by methods involving phase modulating of the optical wave front. Also, the experimental phenomena of optical trapping and transport can be observed. The spiral phase structure embedded into the circular Pearcey beam is responsible for achieving a hollow optical guide channel, and the specially designed phase modulation is intended for guiding the vortex along arbitrarily pre-designed trajectories, which therefore promise the application of guiding the trapped particles along arbitrarily pre-designed trajectories while evading obstacles. We choose the circular Pearcey vortex beam to modulate its trajectory due to its autofocusing property and enhanced intensity contrast, which is conducive to maintaining the energy converging on the brightest ring for a longer propagation distance. The intensity focuses on the ring surrounding the dark area where the phase singularity exists, which contributes to forming an ultralong dark channel, so that the stable trapping of particles and optical guidance are more effective. Compared with Ref. [24], the CPLVB breaks the parabolic trajectory restrictions, exhibiting abruptly autofocusing in the off-axis position and enabling a twisting dark channel spiraling along arbitrary trajectories. The setup of the paper is as follows. In Sec. II, the theoretical model for generating the CPLVB is introduced in detail. Then we give related discussions of three examples including hyperbolic, hyperbolic secant, and parabolic trajectories in Sec. III. In Sec. IV, generation of the CPLVB is realized experimentally and demonstrations about particle trapping and transport are presented. Eventually, conclusions are summarized in Sec. V.

II. THEORETICAL MODEL OF THE CIRCULAR PEARCEY-LIKE VORTEX BEAMS

In the paraxial optical system, the optical beam propagating along the z axis in the free space can be described by the Fresnel diffraction integral [51]

$$u(x, y, z) = \frac{k \exp(ikz)}{i2\pi z} \int \int_{-\infty}^{\infty} u_0(x', y', 0) \times \exp \left\{ \frac{ik}{2z} [(x-x')^2 + (y-y')^2] \right\} dx' dy', \quad (1)$$

TABLE I. Different trajectories and their corresponding functions ($g(Z)$, $h(Z)$).

Trajectory type	$g(Z)$	$h(Z)$
Hyperbolic trajectory	$\sqrt{0.64Z^2 - 32Z + 800} - \sqrt{800}$	0
Hyperbolic secant trajectory	$g(Z) = 8 \operatorname{sech}(\frac{Z-45}{20})$	0
Parabolic trajectory	$g(Z) = \frac{Z^2}{40}$	0

where $k = \frac{2\pi}{\lambda}$ is the wave number and λ denotes the wavelength. The electric field distribution of the CPLVB at the initial plane can be considered as

$$u_0(x, y, 0) = \operatorname{Pe} \left(\xi, -\frac{r}{\chi w_0} \right) T(r) \exp \left[im \arctan \left(\frac{y}{x} \right) \right] \times \exp \left[iQ \left(\frac{x}{w_0}, \frac{y}{w_0} \right) \right], \quad (2)$$

where Pe is the Pearcey integral in terms of $\operatorname{Pe}(x, y) = \int_{-\infty}^{\infty} ds \exp(is^4 + is^2y + isx)$ [52], ξ is a constant, the radial distance satisfies $r = \sqrt{x^2 + y^2}$, χ stands for the spatial distribution factor determining the intensity distributions of the incident light and the focal position, w_0 represents the normalized scaling factor, and $T(r) = \begin{cases} 1, & r < r_t \\ 0, & r \geq r_t \end{cases}$ ensures that the total conveyed power $\int \int_{-\infty}^{\infty} |u_0(x, y, 0)|^2 dx dy$ is finite [5]. m is the topological charges of the OVVs whose sign determines the handedness of the helix. The phase $Q(\frac{x}{w_0}, \frac{y}{w_0})$ is responsible for modulating the beam into pre-designed trajectories relying on the given function [$g(Z)$, $h(Z)$], which can be expressed as [53]

$$Q \left(\frac{x}{w_0}, \frac{y}{w_0} \right) = \frac{1}{2} \int_0^Z \{ [g'(\tau)]^2 + [h'(\tau)]^2 - \gamma^2 \} d\tau - \frac{[g(Z) - x/w_0]^2 + [h(Z) - y/w_0]^2}{2Z}, \quad (3)$$

where γ indicates the normalized transverse wave number, and $g'(\tau)$ and $h'(\tau)$ are the first derivatives of $g(\tau)$ and $h(\tau)$. For computing the phase $Q(\frac{x}{w_0}, \frac{y}{w_0})$, we should solve the equation $(\gamma Z)^2 = [\frac{x}{w_0} - g(Z) + Zg'(Z)]^2 + [\frac{y}{w_0} - h(Z) + Zh'(Z)]^2$ for Z . Since there are no analytical solutions of Eq. (3), we utilize MATLAB to calculate the three-dimensional optical light fields of the CPLVB along arbitrary trajectories.

In this paper, we set the parameters $\lambda = 532$ nm, $w_0 = 0.016$ mm, $\xi = 0$, $\chi = 6$, $r_t = 1.58$ mm, $\gamma = 1$, and $z_e = \frac{kw_0^2}{2}$ indicates the Rayleigh distance. Following the aforementioned procedure of designing phase Q to control the CPLVB along arbitrary trajectories, we give three examples including a hyperbolic trajectory, a hyperbolic secant trajectory, and a parabolic trajectory in Table I. In the above three cases, we focus on the situation of trajectories lying on the x - z plane due to symmetry, so we consider $h(Z) = 0$.

The complete process of generating phases of the CPLVB propagating along specially designed trajectories is illustrated in Fig. 1. The phase of the circular Pearcey beam and the spiral phase are presented in Figs. 1(a) and 1(b), respectively. The phases Q as shown in Figs. 1(c1)–1(c3) can be obtained by

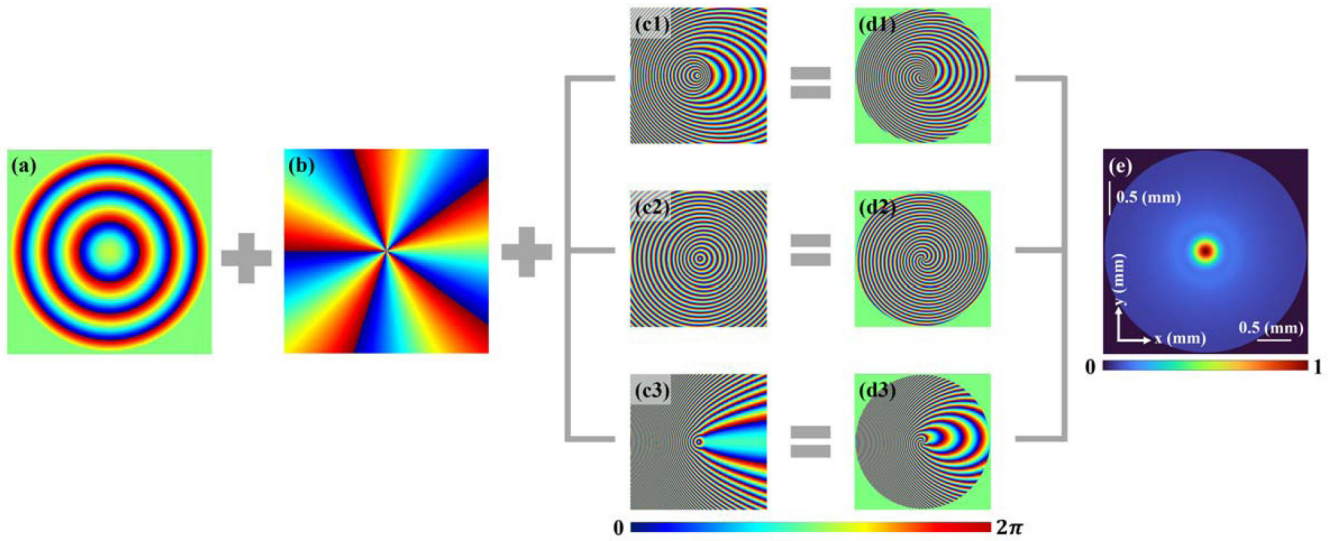


FIG. 1. Process of generating the phase distributions of the CPLVB. (a) The phase of the circular Pearcey beam; (b) the spiral phase with $m = 5$; (c1)—(c3) the phases Q respectively corresponding to the hyperbolic trajectory, hyperbolic secant trajectory, and parabolic trajectory; (d1)—(d3) the phases of the CPLVB; (e) normalized intensity distributions at the initial plane.

substituting the given function $[g(Z), h(Z)]$ to Eq. (3), which are utilized to modulate the wave front formed by embedding the spiral phase into the circular Pearcey beam. As a result, the phases of input wave fronts in Figs. 1(d1)–1(d3) direct conical bundles of rays emanating from a series of circles at the initial plane to create a continuous focal curve with predesigned shape written as $[g(Z), h(Z), Z]$. Any point on this curve is the apex of these ray cones whose interference leads to a circular Pearcey-like vortex pattern along a specified transmission path. In Fig. 1(e), it is found that the initial patterns form a series of concentric ring structures.

III. NUMERICAL SIMULATIONS AND DISCUSSIONS

At first, we consider the scenario in which case the CPLVB propagates along a hyperbolic trajectory. As can be seen from Figs. 2(a1) and 2(a2), we indeed notice that the OVs guided by the circular Pearcey-like beam follow a hyperbolic path, exhibiting an ultralong hollow optical channel. The CPLVB initially accelerates downwards and then deflects to perform an oblique projectile motion upwards. During propagation, the CPLVB forms an annular structure, and then gradually deviates from the center relying on the phase modulation Q [Fig. 1(c1)], which leads to the intensity profiles in an asymmetric fashion. Afterwards, the dark region shrinks and the vortex is antiexpanding on account of the abruptly autofocusing effect. The helix phase interferences between a plane wave and the CPLVB at the desired propagation distance can be used in detecting and measuring the existence of vortices [54,55]. As depicted in Figs. 2(a3) and 2(a4), the location of the vortex singularity is marked with red circles. Note that spiral stripes extend outward from the vortex singularity where the interference fringes with bifurcation form. As a result, the OVs guided by the beam follow a hyperbolic trail with the assistance of the specially designed phase modulation Q , which elucidates the formation of the twisting dark channel. Next, we model another scenario that the CPLVB

travels along a hyperbolic secant orbit which is modulated by the phase distribution in Fig. 1(c2). Figures 2(b1) and 2(b2) refer to a beam that initially performs ascending movement and then deflects to accelerate downwards; in the end the beam returns to a straight line parallel to the optical axis. As described in Figs. 2(b3) and 2(b4), it is worth mentioning that the transverse deviation of vortex resulting from the inclusion of the topological phase structure interacting with the modulated beams shapes a twisting hollow channel spiraling along a hyperbolic secant line. In addition, the last example that the CPLVB follows a parabolic trail is illustrated in Figs. 2(c1) and 2(c2). The CPLVB inherits the abruptly autofocusing property from the circular Pearcey beam, shaping a parabolic bottle-like structure. It is noticeable that the head of such bending bottle-like structure is situated at the initial plane, and the bottom is located at the autofocusing plane, which serves as a light wall to confine the particles within the dark regions enclosed by high intensity. Furthermore, in contrast to Figs. 2(a2) and 2(b2), the length of the dark hollow channel is much shorter, which is fit for transporting particles at a shorter distance. In Figs. 2(c3) and 2(c4), it is clearly observed that the OVs can be guided to accelerate along the parabolic trajectory due to the interplay between the spiral phase and the phase pattern in Fig. 1(c3) which is utilized to generate and regulate the transverse self-accelerating behavior. The number of spiral stripes and the morphology of the bifurcation in the helix phase interferences are related to the topological charges and the OAM of the beam [10]. The reason why the OVs superimposed on the beam could move on arbitrary trajectories is that the intensity gradient of the beam serves as the driving force for the motion of the singularity point. Hence, as for the trapped particles with higher refractive indices than that of their surroundings, they would be trapped in a doughnut structure where the intensity focuses. The absorption of light and the OAM transferred from the helically phased beam to particles result in the rotation motion of particles [56]. In terms of the particles with lower refractive indices than that

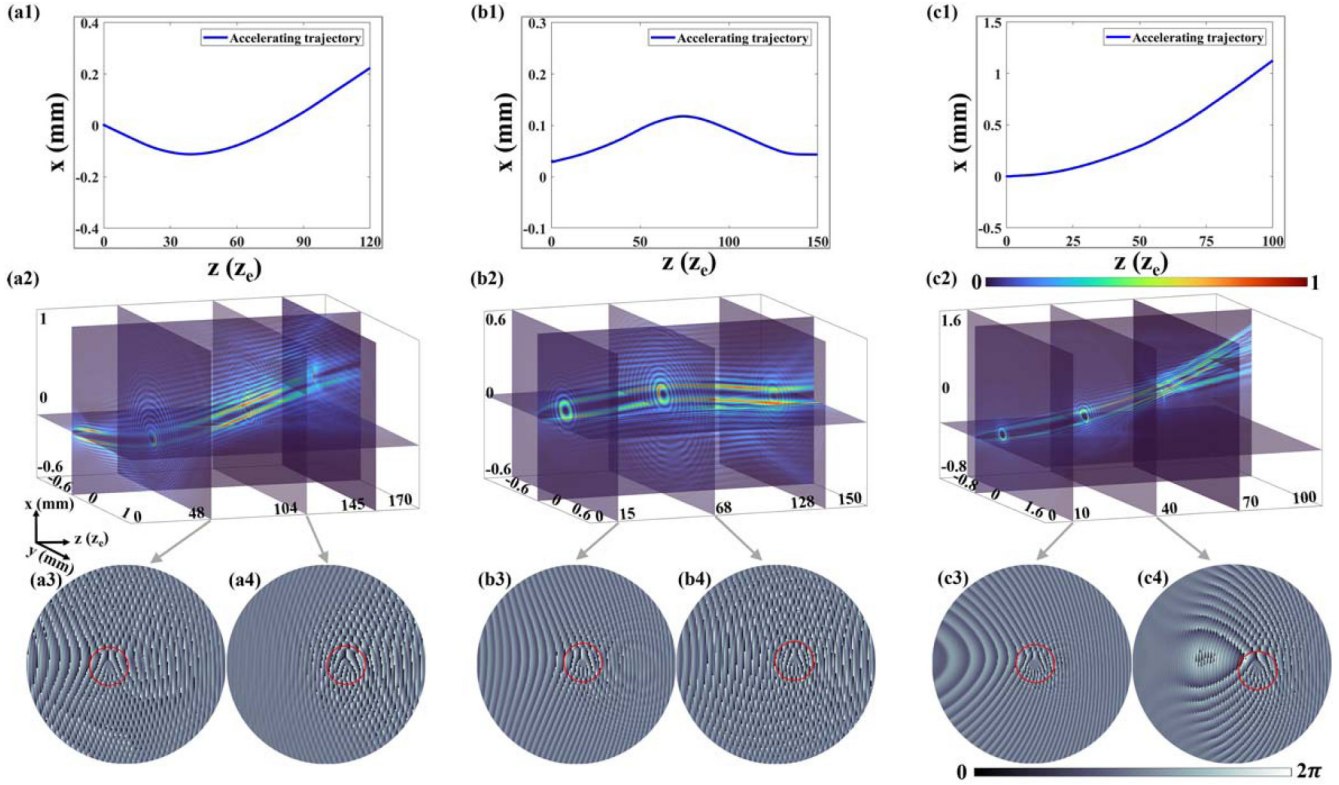


FIG. 2. Numerical results showing the CPLVB propagating in the free space along arbitrary trajectories. (a1)–(a4) The accelerating trajectory curves (a1), the slice diagrams (a2), and the phase interference patterns [(a3) and (a4)] of the CPLVB propagating along a hyperbolic trajectory with $m = 4$; (b1)–(b4) the accelerating trajectory curves (b1), the slice diagrams (b2), and the phase interference patterns [(b3) and (b4)] of the CPLVB moving on a hyperbolic secant trajectory with $m = 3$; (c1)–(c4) the accelerating trajectory curves (c1), the slice diagrams (c2), and the phase interference patterns [(c3) and (c4)] of the CPLVB accelerating along a parabolic trajectory with $m = 5$. The location of the vortex singularity is marked with red circles.

of their surroundings, the CPLVB carrying the OV forms an energy potential well, which suggests that the particles can be repelled from the high light wall and transport in a dark channel [43]. That means such optical structure is expected to be applied in guiding particles along arbitrary trajectories.

IV. EXPERIMENTAL SETUP AND DEMONSTRATIONS FOR PARTICLE GUIDANCE

The experimental setup for generating the CPLVB and demonstrating the particle trapping is sketched in Fig. 3, which utilizes the principle of holographic imaging. The designed phase masks with interference fringes containing both amplitude and phase information of the CPLVB are programmed to the spatial light modulator (SLM) through a computer [57]. A Gaussian laser mode emitted from a $\lambda = 532$ nm laser is orderly sent through a half-wave plate and a Gran prism for the purpose of controlling the beam power and satisfying the SLM requirements for the polarization direction of the incident light [58]. After being collimated and expanded by the beam expander, the beam is reflected from a mirror to the SLM to carry the encoded information. Then the $4f$ filter system consisting of two lenses (L3, L4) and an aperture is responsible for selecting only the positive first-order diffraction component. The beam passing through

the beam splitter is divided into two parts. One is sent into the charge-coupled device (CCD) to record intensity cross sections, and the other is directed to a high-numerical-aperture oil-immersion objective ($100\times$, $NA = 1.25$) by a dichroic mirror (DM). The DM and the optical filter are used to prevent the CPLVB from entering the complementary metal-oxide semiconductor (CMOS) camera while allowing white light to pass through. The sample contains silica particles suspended in the distilled water solution and sandwiched between two thin glass plates, which is placed on a three-dimensional adjustable displacement platform [38]. With the help of the delay system [59] composed by four mirrors fixed on a translation stage, the optical path is controllable so that the transverse intensity evolutions at different z -axial locations can be obtained by the CCD, and the image plane of the objective enables it to be varied for generating desired light patterns. Different from the proposed method that moves the sample to visualize the particle trapping at various cross sections of the targeting beam [6], such a delay system seems more convenient in regulating the experimental system and reduces the oscillation of particles caused by the instable movement of sample. A white light source (WLS) is adopted to illuminate the sample, so imaging of the particle trapping situation is achieved by the CMOS camera.

The desired phase masks shown in Figs. 4(a1) 4(b1), and 4(c1) can be obtained by interfering the initial field of

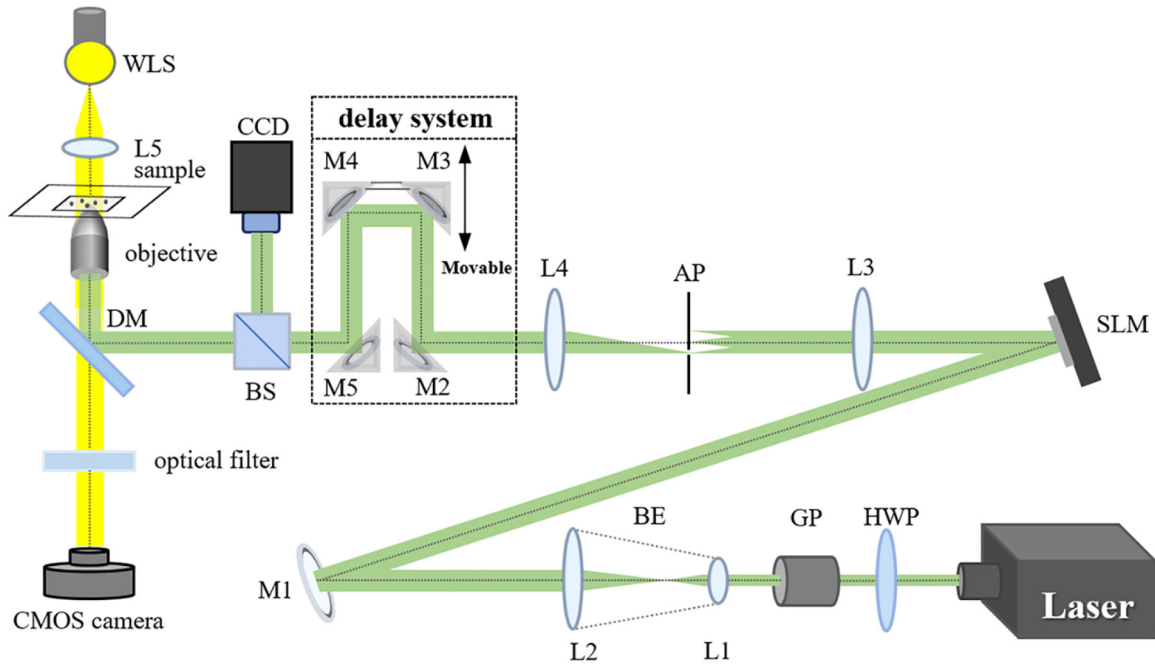


FIG. 3. Schematic of the experimental setup for generating the CPLVB and observing the particle trapping. Laser ($\lambda = 532$ nm); HWP, half-wave plate; GP, Gran prism; BE, beam expander (consisting of two lenses L1, L2); L1–L5, lenses; M1–M5, mirrors; SLM, spatial light modulator (Santec SLM-200, 1920×1080 pixels); AP, aperture; BS, beam splitter with the splitting ratio of 9:1; CCD, charge-coupled device (BeamPro 11.11, 2048×2048 pixels); DM, dichroic mirror; WLS, white light source; CMOS camera, complementary metal oxide semiconductor camera.

the CPLVB with a plane wave, which are given by

$$\psi_{\text{SLM}} = |1 + u_0 \exp(i2\pi f_x x)|^2, \quad (4)$$

where f_x represents the grating frequency and controls the diffraction angle of the beam reflected from the SLM in the x direction. We can adjust the value of f_x to avoid the overlapping of diffraction fringes on the spectrum plane, so that the positive first-order fringe can be selected by the $4f$ filter system. The grating depth and spatial phase delay of the phase masks determine the amplitude and the phase information of the CPLVB, respectively [60]. After imposing the phase masks onto the SLM, the CPLVB is generated by the experimental setup in Fig. 3 and the experimental snapshots are measured by the CCD. We can observe the corresponding transverse intensity evolutions by steadily moving the mirrors (M3, M4) in the delay system. When the motion trajectory is a hyperbolic line presented in Figs. 4(a2)–4(a4), the CPLVB initially forms an annular pattern and gradually deviates from the center along the positive x -axial direction. The area of the dark core becomes narrow due to the autofocusing process. As for the beam moving on a hyperbolic secant trajectory shown in Figs. 4(b2)–4(b4), the doughnut shape is formed at the initial propagation stage, and with the ascending propagation distances the crescentlike mode gets rotated because of the OAM associated with the helical wave-front structure and phase singularity. In the case of the beam traveling along a parabolic trail in Figs. 4(c2)–4(c4), the right half of the ring accelerates faster along the positive x -axial direction away from the center while the left half is slower, demonstrating the self-bending behavior. Finally, the beam evolves into the

bottom of a parabolic bottle-like structure due to the abruptly autofocusing trait.

In order to validate that the CPLVB can be applied to an optical tweezer system to achieve particle manipulation, we choose the case that the beam propagates along the hyperbolic secant trajectory to construct a twisting hollow channel. The $4 \mu\text{m}$ silica particles we used are much larger than the wavelength, so the radiation pressures exerted on such micron-sized particles can be described by a ray optics model [44]. Additionally, the refractive index of silica particles in a fluid environment is higher than that of surroundings so that the gradient force drags particles into regions of high intensity [61]. As depicted in Fig. 5(a1), the beam continues to perform a ringlike distribution during propagation, which can guide the particles with a ring pattern formed to spiral forward along a hyperbolic secant orbit. By translating the delay system, the trapping beam profile can be adjusted. The laser output power is increased to 4.8 W, which is capable of intensifying the gradient force to defeat the Brownian motion. As depicted in Figs. 5(b1)–5(b5) which perform the trapping process, the particles subjected to a vortex trap are gradually trapped onto the annulus of the peak intensity under the action of the gradient force. The particle circled by a solid yellow circle located at the position of the vortex singularity [Fig. 5(b4)] is repelled and ultimately a ring pattern is presented [Fig. 5(b5)] in order to match the transverse distribution in Figs. 5(a2) and 5(a3). When we slightly move the sample stage in the x - and y -axial planes, the particles which form a ring shape are trapped very stably. Besides stable trapping, the spinning motion of particles is another appealing aspect of optical manipulation which is exhibited in

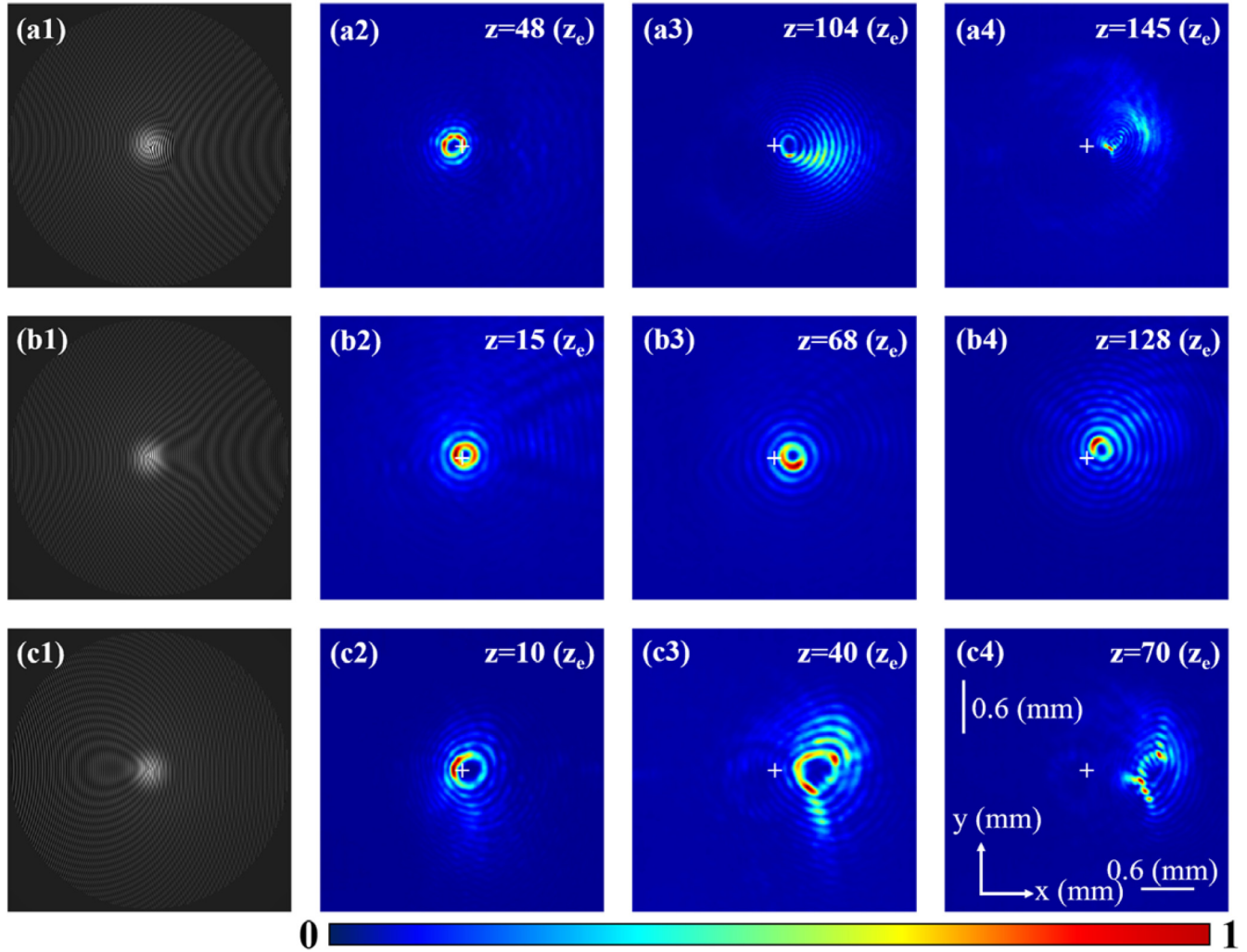


FIG. 4. (a1)–(a4) Phase mask (a1) and experimental snapshots of transverse intensity patterns [(a2)–(a4)] of the CPLVB propagating along a hyperbolic trajectory with $m = 4$, $f_x = 8 \text{ mm}^{-1}$; (b1)–(b4) phase mask (b1) and measured transverse intensity patterns [(b2)–(b4)] of the CPLVB moving on a hyperbolic secant trajectory with $m = 3$, $f_x = 10 \text{ mm}^{-1}$; (c1)–(c4) phase mask (c1) and recorded transverse intensity patterns [(c2)–(c4)] of the CPLVB accelerating along a parabolic trajectory with $m = 5$, $f_x = 10 \text{ mm}^{-1}$. The white cross marks the center.

Figs. 5(c1)–5(c5). The rotation process is shown in the video file [62]. The solid yellow circles and the white arrows depict the rotation trajectory of particles. The interaction and the OAM transfer between the CPLVB with a phase singularity and the trapped particles lead to the anticlockwise rotation of particles on a circular orbit.

Furthermore, the continuous experimental setup shown in Fig. 6(a) is placed after the $4f$ filter system which takes the place of the optical tweezer system in Fig. 3. The function of the reverse telescope consisting of two lenses (L6, L7) is to downsize the beam to match the typical size of the light-absorbing particles used in the experiment. Particle transport in air is visualized by generating the CPLVB along the parabolic trajectory. The optical bottle-like structure is constructed into a glass cuvette which contributes to attenuating ambient perturbations [43]. In this experiment, the transverse size of the dark area in the body of the bottle-like structure we implement here is about $28 \mu\text{m}$. The light-absorbing particles we used are mesocarbon particles of median sizes

$D_{50} = 23.828 \mu\text{m}$ and the laser output power is approximately 1 W. Based on the photophoretic force, such a structure generated at the image focal plane of L2 in Fig. 3 can be employed to trap and transport mesocarbon particles within the dark regions surrounded by the high-intensity barrier. The physical mechanism is that the light-absorbing particles illuminated by a laser beam have a nonuniform temperature distribution and collisions of gas molecules with the heated particle surface give rise to the photophoretic force exerted on the particles to repel them from high-intensity regions [63]. After putting mesocarbon particles in the glass cuvette, we shake the glass cuvette to fill it with the floating mesocarbon particles. The side views of the scattered light from the trapped particles are captured by a camera to monitor the trapping procedure, as seen in Figs. 6(d1) and 6(d2). It is found that multiple particles are restricted in the dark hollow body of the bottle-like structure but with a high-frequency oscillation due to the particles susceptible to ambient perturbations. Additionally, the particles are guided to transport forward along the parabolic trajectory in Fig. 6(c) because collisions

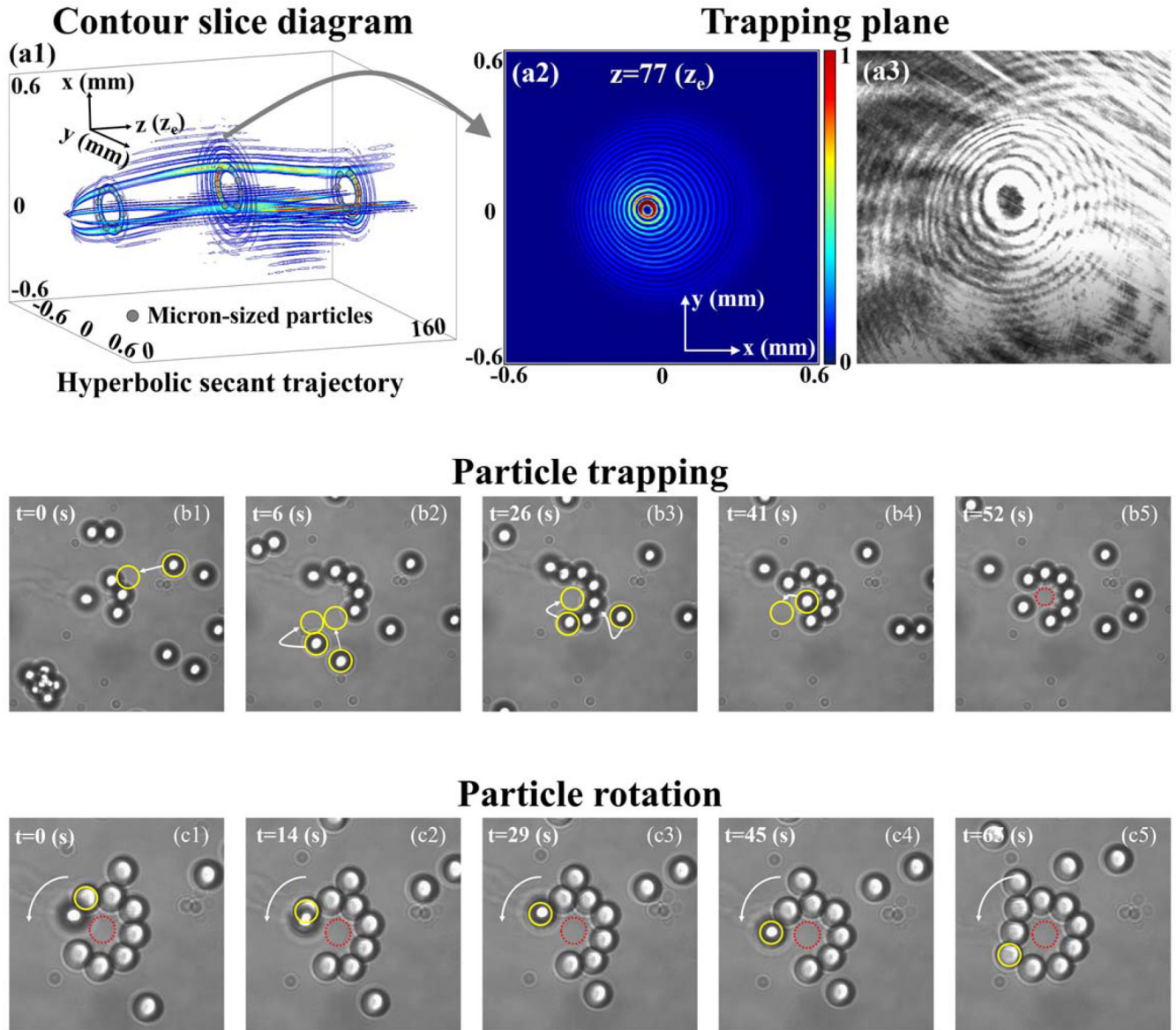


FIG. 5. Experimental verification of particle trapping and rotation using the CPLVB moving on a hyperbolic secant line ($m = 7$). (a1) Contour slice diagram of the CPLVB propagating along a hyperbolic secant trajectory; (a2) numerical simulation of the trapping plane; (a3) imaging plane of the objective in experiment; (b1)–(b5) snapshots of particles trapped at the trapping plane (a3); and (c1)–(c5) snapshots of particle rotation; the rotation process is shown in the video file (see Supplemental Material [62], which is sped up). The dashed red circles mark the location of the vortex singularity. The white arrows depict the direction of motion of the particles circled by solid yellow circles.

of gas molecules with the particle surface on the illuminated side are stronger than that on the other side [63]. After a few seconds, it is discovered that the particles touching the high light wall, which is considered as the bottom of the bottle-like structure as discussed earlier, scatter light and cause a stable and bright spot in Fig. 6(d2). Therefore, the OV's guided by the circular Pearcey-like beam enable light-absorbing particles to transport along pre-designed trajectories.

V. CONCLUSION

In summary, the CPLVB applied in particle trapping is proposed numerically and generated experimentally, which

is the combination of the circular Pearcey beam with the spiral phase and the modulated phase Q of the pre-designed trajectory. Through phase modulating the optical wave front, three examples including hyperbolic, hyperbolic secant, and parabolic trajectories are discussed. When the CPLVB moves on hyperbolic and hyperbolic secant trajectories, an ultra-long hollow optical channel is generated. As for the case that the CPLVB travels along the parabolic trajectory, a parabolic bottle-like structure is constructed. Notably, the experimental setup for generating the CPLVB and observing the particle guidance is exhibited. The experimental observations of transverse intensity patterns are consistent with the numerical simulations. The stable trapping and rotation motion of particles can be achieved by considering the

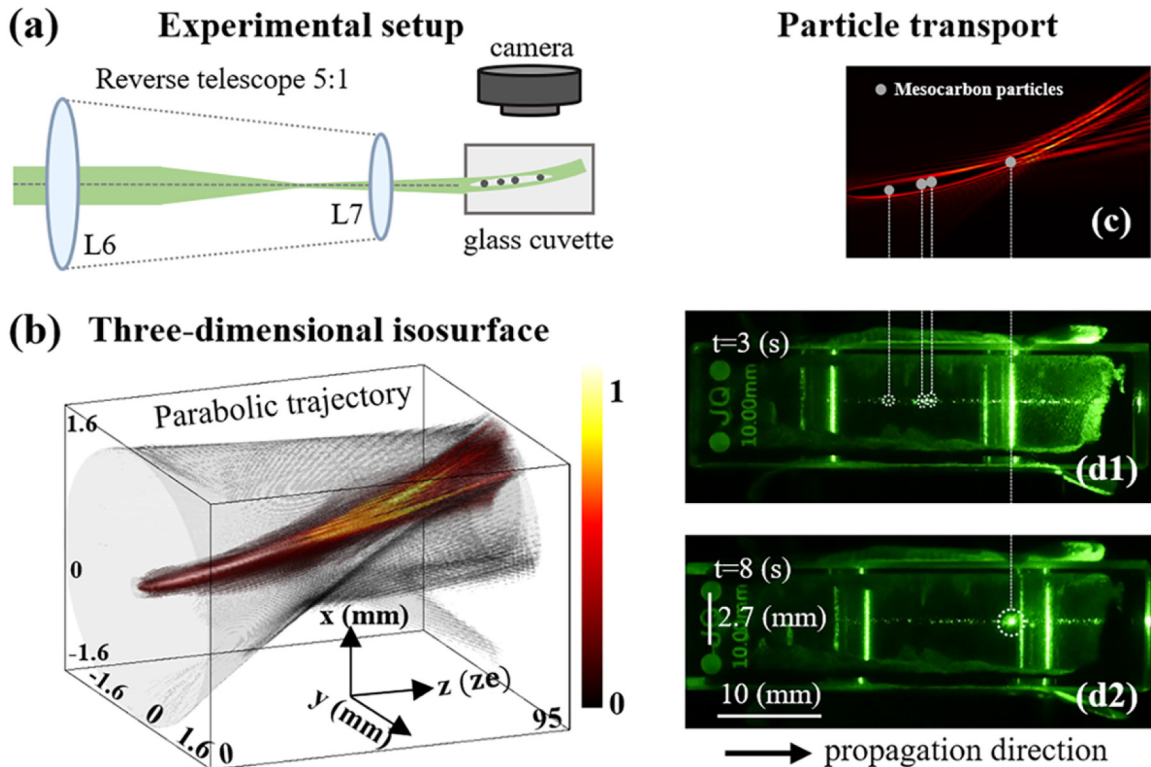


FIG. 6. Experimental verification of guiding particles along the parabolic trajectory $[(g(Z), h(Z)) = (\frac{Z^2}{30}, 0)]$ with $m = 5$; (a) schematic of the continuous experimental setup after the $4f$ filter system in Fig. 3; L6, L7, lenses; (b) three-dimensional isosurface of the CPLVB propagating along the parabolic trajectory in the glass cuvette (10 mm \times 10 mm \times 40 mm); (c) numerical side view of the CPLVB propagating along the parabolic trajectory; (d1), (d2) photographs taken at the side of the glass cuvette to capture the particle motion. The white dashed circles mark the particles trapped within the parabolic bottle-like structure.

example that the beam propagates along the hyperbolic secant trajectory forming a twisting hollow channel. Utilizing the parabolic bottle-like structure to constrain the light-absorbing particles within the dark regions surrounded by the high-intensity barrier provides an intuitive demonstration of guiding particles along predefined trajectories. The results concluded above may better facilitate applications for wavefront control, optical guidance of particles, and flexible optical manipulation.

Data underlying the results presented in this paper are not publicly available at this time but may be obtained from the authors upon reasonable request.

ACKNOWLEDGMENTS

The authors acknowledge support from National Natural Science Foundation of China (Grants No. 12174122 and No. 11775083); Guangdong provincial Natural Science Foundation of China (Grant No. 2022A1515011482); Science and Technology Program of Guangzhou (Grant No. 2019050001); the Extracurricular Scientific Program of School of Information and Optoelectronic Science and Engineering, South China Normal University (Grant No. 21GDKB02); and Special Funds for the Cultivation of Guangdong College Students Scientific and Technological Innovation (“Climbing Program” Special Funds; pdjh2022a0129).

The authors declare no conflict of interest.

- [1] N. K. Efremidis and D. N. Christodoulides, Abruptly autofocusing waves, *Opt. Lett.* **35**, 4045 (2010).
- [2] D. G. Papazoglou, N. K. Efremidis, D. N. Christodoulides, and S. Tzortzakis, Observation of abruptly autofocusing waves, *Opt. Lett.* **36**, 1842 (2011).
- [3] I. Chremmos, N. K. Efremidis, and D. N. Christodoulides, Pre-engineered abruptly autofocusing beams, *Opt. Lett.* **36**, 1890 (2011).
- [4] J. L. Zhuang, D. M. Deng, X. Y. Chen, F. Zhao, X. Peng, D. D. Li, and L. P. Zhang, Spatiotemporal sharply autofocused dual-

Airy-ring Airy Gaussian vortex wave packets, *Opt. Lett.* **43**, 222 (2018).

- [5] X. Y. Chen, D. M. Deng, J. L. Zhuang, X. Peng, D. D. Li, L. P. Zhang, F. Zhao, X. B. Yang, H. Z. Liu, and G. H. Wang, Focusing properties of circle Pearcey beams, *Opt. Lett.* **43**, 3626 (2018).
- [6] P. Zhang, J. Prakash, Z. Zhang, M. S. Mills, N. K. Efremidis, D. N. Christodoulides, and Z. G. Chen, Trapping and guiding microparticles with morphing autofocusing Airy beams, *Opt. Lett.* **36**, 2883 (2011).

- [7] M. Manousidaki, D. G. Papazoglou, M. Farsari, and S. Tzortzakis, Abruptly autofocusing beams enable advanced multiscale photo-polymerization, *Optica* **3**, 525 (2016).
- [8] K. H. Chen, H. X. Qiu, Y. Wu, Z. J. Lin, H. Q. Huang, L. L. Shui, H. Z. Liu, D. M. Deng, and Z. G. Chen, Generation and control of dynamically tunable circular Pearcey beams with annular spiral-zone phase, *Sci. China: Phys., Mech. Astron.* **64**, 104211 (2021).
- [9] L. Xin, Z. Q. Li, Y. E. Monfared, C. H. Liang, F. Wang, B. J. Hoenders, Y. J. Cai, and P. J. Ma, Flexible autofocusing properties of ring Pearcey beams by means of a cross phase, *Opt. Lett.* **46**, 70 (2021).
- [10] Y. J. Shen, X. J. Wang, Z. W. Xie, C. J. Min, X. Fu, Q. Liu, M. L. Gong, and X. C. Yuan, Optical vortices 30 years on: OAM manipulation from topological charge to multiple singularities, *Light: Sci. Appl.* **8**, 90 (2019).
- [11] G. Gibson, J. Courtial, M. J. Padgett, M. Vasnetsov, V. Pas'ko, S. M. Barnett, and S. Franke-Arnold, Free-space information transfer using light beams carrying orbital angular momentum, *Opt. Express* **12**, 5448 (2004).
- [12] K. T. Gahagan and G. A. Swartzlander, Optical vortex trapping of particles, *Opt. Lett.* **21**, 827 (1996).
- [13] M. Mirhosseini, O. S. Magaña-Loaiza-Loaiza, M. N. O'Sullivan, B. Rodenburg, M. Malik, M. P. J. Lavery, M. J. Padgett, D. J. Gauthier, and R. W. Boyd, High-dimensional quantum cryptography with twisted light, *New J. Phys.* **17**, 033033 (1996).
- [14] L. Allen, M. W. Beijersbergen, R. J. C. Spreeuw, and J. P. Woerdman, Orbital angular momentum of light and the transformation of Laguerre-Gaussian laser modes, *Phys. Rev. A* **45**, 8185 (1992).
- [15] D. G. Grier, A revolution in optical manipulation, *Nature (London)* **424**, 810 (2003).
- [16] J. E. Curtis and D. G. Grier, Structure of Optical Vortices, *Phys. Rev. Lett.* **90**, 133901 (2003).
- [17] N. B. Simpson, L. Allen, and M. J. Padgett, Optical tweezers and optical spanners with Laguerre-Gaussian modes, *J. Mod. Opt.* **43**, 2485 (1996).
- [18] I. Zeylikovich and A. Nikitin, The formation and propagation of Mathieu-Gauss type spatial structures on diffraction of a multi segment-shaped laser beam, *Eur. Phys. J. D* **74**, 182 (2020).
- [19] X. X. Chu, Q. Sun, J. Wang, P. Lu, W. K. Xie, and X. J. Xu, Generating a Bessel-Gaussian beam for the application in optical engineering, *Sci. Rep.* **5**, 18665 (2016).
- [20] Y. Chen, Z. X. Fang, Y. X. Ren, L. Gong, and R. D. Lu, Generation and characterization of a perfect vortex beam with a large topological charge through a digital micromirror device, *Appl. Opt.* **54**, 8030 (2015).
- [21] R. P. Chen and C. Q. Dai, Three-dimensional vector solitons and their stabilities in a Kerr medium with spatially inhomogeneous nonlinearity and transverse modulation, *Nonlinear Dyn.* **88**, 2807 (2017).
- [22] L. Y. Zhu, Y. Chen, Z. X. Fang, W. P. Ding, and R. D. Lu, Experimental demonstration and investigation of vortex circular Pearcey beams in a dynamically shaped fashion, *Opt. Express* **29**, 19819 (2021).
- [23] P. Li, S. Liu, T. Peng, G. F. Xie, X. T. Gan, and J. L. Zhao, Spiral autofocusing Airy beams carrying power-exponent-phase vortices, *Opt. Express* **22**, 7598 (2014).
- [24] Z. X. Fang, Y. Chen, Y. X. Ren, L. Gong, R. D. Lu, A. Q. Zhang, H. Z. Zhao, and P. Wang, Interplay between topological phase and self-acceleration in a vortex symmetric Airy beam, *Opt. Express* **26**, 7324 (2018).
- [25] G. A. Siviloglou and D. N. Christodoulides, Accelerating finite energy Airy beams, *Opt. Lett.* **32**, 979 (2007).
- [26] G. A. Siviloglou, J. Broky, A. Dogariu, and D. N. Christodoulides, Observation of Accelerating Airy Beams, *Phys. Rev. Lett.* **99**, 213901 (2007).
- [27] I. Kaminer, R. Bekenstein, J. Nemirovsky, and M. Segev, Non-diffracting Accelerating Wave Packets of Maxwell's Equations, *Phys. Rev. Lett.* **108**, 163901 (2012).
- [28] P. Zhang, Y. Hu, T. Li, D. Cannan, X. Yin, R. Morandotti, Z. Chen, and X. Zhang, Nonparaxial Mathieu and Weber Accelerating Beams, *Phys. Rev. Lett.* **109**, 193901 (2012).
- [29] Y. Hu, D. Bongiovanni, Z. G. Chen, and R. Morandotti, Periodic self-accelerating beams by combined phase and amplitude modulation in the Fourier space, *Opt. Lett.* **38**, 3387 (2013).
- [30] Y. Hu, D. Bongiovanni, Z. G. Chen, and R. Morandotti, Multipath multicomponent self-accelerating beams through spectrum-engineered position mapping, *Phys. Rev. A* **88**, 043809 (2013).
- [31] Y. X. Qian, S. T. Zhang, and Z. J. Ren, Generation of Accelerating beams along arbitrary trajectories, *Ann. Phys. (Berlin, Ger.)* **531**, 1800473 (2019).
- [32] N. K. Efremidis, Airy trajectory engineering in dynamic linear index potentials, *Opt. Lett.* **36**, 3006 (2011).
- [33] K. Y. Zhan, Z. D. Yang, B. Liu, X. F. Xu, Z. Y. Jiao, and Y. L. Jia, Propagations of Airy beams and nonlinear accelerating optical beams in photorefractive crystals with asymmetric nonlocality, *Ann. Phys. (Berlin, Ger.)* **530**, 1800033 (2018).
- [34] X. Y. Wang, H. Y. Chen, H. Liu, L. Xu, C. Sheng, and S. N. Zhu, Self-Focusing and the Talbot Effect in Conformal Transformation Optics, *Phys. Rev. Lett.* **119**, 033902 (2017).
- [35] A. Ashkin, Acceleration and Trapping of Particles by Radiation Pressure, *Phys. Rev. Lett.* **24**, 156 (1970).
- [36] A. Ashkin, Trapping of Atoms by Resonance Radiation Pressure, *Phys. Rev. Lett.* **40**, 729 (1978).
- [37] M. Dienerowitz, M. Mazilu, and K. Dholakia, Optical manipulation of nanoparticles: A review, *J. Nanophotonics* **2**, 021875 (2008).
- [38] P. Zhang, D. Hernandez, D. Cannan, Y. Hu, S. Fardad, S. Huang, J. C. Chen, D. N. Christodoulides, and Z. G. Chen, Trapping and rotating microparticles and bacteria with moiré-based optical propelling beams, *Biomed. Opt. Express* **3**, 1891 (2012).
- [39] K. C. Neuman, T. Lionnet, and J.-F. Allemand, Single-molecule micromanipulation techniques, *Annu. Rev. Mater. Res.* **37**, 33 (2007).
- [40] A. Ashkin, J. M. Dziedzic, and T. Yamane, Optical trapping and manipulation of single cells using infrared laser beams, *Nature (London)* **330**, 769 (1987).
- [41] H. P. Wang, L. Q. Tang, J. Ma, H. W. Hao, X. Y. Zheng, D. H. Song, Y. Hu, Y. G. Li, and Z. G. Chen, Optical clearing and shielding with fan-shaped vortex beams, *APL Photonics* **5**, 016102 (2020).
- [42] Y. J. Yang, Y. X. Ren, M. Z. Chen, Y. Arita, and C. Rosales-Guzmán, Optical trapping with structured light: A review, *Adv. Photonics* **3**, 034001 (2021).
- [43] A. Turpin, V. Shvedov, C. Hnatovsky, Y. V. Loiko, J. Mompart, and W. Krolikowski, Optical vault: A reconfigurable bottle

- beam based on conical refraction of light, *Opt. Express* **21**, 26335 (2013).
- [44] P. Zemánek, G. Volpe, A. Jonáš, and O. Brzobohatý, Perspective on light-induced transport of particles: From optical forces to phoretic motion, *Adv. Opt. Photonics* **11**, 577 (2019).
- [45] Y. Roichman, B. Sun, Y. Roichman, J. Amato-Grill, and D. G. Grier, Optical Forces Arising from Phase Gradients, *Phys. Rev. Lett.* **100**, 013602 (2008).
- [46] V. G. Shvedov, A. S. Desyatnikov, A. V. Rode, W. Krolikowski, and Y. S. Kivshar, Optical guiding of absorbing nanoclusters in air, *Opt. Express* **17**, 5743 (2009).
- [47] A. B. Pluchino and S. Arnold, Comprehensive model of the photophoretic force on a spherical microparticle, *Opt. Lett.* **10**, 261 (1985).
- [48] P. Zhang, Z. Zhang, J. Prakash, S. Huang, D. Hernandez, M. Salazar, D. N. Christodoulides, and Z. G. Chen, Trapping and transporting aerosols with a single optical bottle beam generated by moiré techniques, *Opt. Lett.* **36**, 1491 (2011).
- [49] A. S. Desyatnikov, V. G. Shvedov, A. V. Rode, W. Krolikowski, and Y. S. Kivshar, Photophoretic manipulation of absorbing aerosol particles with vortex beams: Theory versus experiment, *Opt. Express* **17**, 8201 (2009).
- [50] V. Shvedov, A. R. Davoyan, C. Hnatovsky, N. Engheta, and W. Krolikowski, A long-range polarization-controlled optical tractor beam, *Nat. Photonics* **8**, 846 (2014).
- [51] A. E. Siegman, *Lasers* (University Science Books, Melville, NY, 1986).
- [52] J. D. Ring, J. Lindberg, A. Mourka, M. Mazilu, K. Dholakia, and M. R. Dennis, Auto-focusing and self-healing of Pearcey beams, *Opt. Express* **20**, 18955 (2012).
- [53] I. D. Chremmos, Z. G. Chen, D. N. Christodoulides, and N. K. Efremidis, Bessel-like optical beams with arbitrary trajectories, *Opt. Lett.* **37**, 5003 (2012).
- [54] A. M. Yao and M. J. Padgett, Orbital angular momentum: Origins, behavior and applications, *Adv. Opt. Photonics* **3**, 161 (2011).
- [55] W. M. Lee and X-C. Yuan, Experimental observation of ‘pure helical phase’ interference using moiré fringes generated from holograms with dislocations, *J. Opt. A: Pure Appl. Opt.* **6**, 482 (2004).
- [56] H. He, M. E. J. Friese, N. R. Heckenberg, and H. Rubinsztein-Dunlop, Direct Observation of Transfer of Angular Momentum to Absorptive Particles from a Laser Beam with a Phase Singularity, *Phys. Rev. Lett.* **75**, 826 (1995).
- [57] I. S. V. Yepes, T. A. Vieira, R. A. B. Suarez, S. R. C. Fernandez, and M. R. R. Gesualdi, Phase and intensity analysis of non-diffracting beams via digital holography, *Opt. Commun.* **437**, 121 (2019).
- [58] X. Y. Zhou, Z. H. Pang, and D. M. Zhao, Generalized ring Pearcey beams with tunable autofocusing properties, *Ann. Phys. (Berlin, Ger.)* **533**, 2100110 (2021).
- [59] W. X. Yan, Y. Gao, Z. Yuan, Z. Wang, Z. C. Ren, X. L. Wang, J. P. Ding, and H. T. Wang, Non-diffracting and self-accelerating Bessel beams with on-demand tailored intensity profiles along arbitrary trajectories, *Opt. Lett.* **46**, 1494 (2021).
- [60] X. Liu, Y. E. Monfared, R. Pan, P. Ma, and C. Liang, Experimental realization of scalar and vector perfect Laguerre–Gaussian beams, *Appl. Phys. Lett.* **119**, 021105 (2021).
- [61] V. Bobkova, J. Stegemann, R. Droop, E. Otte, and Cornelia Denz, Optical grinder: Sorting of trapped particles by orbital angular momentum, *Opt. Express* **29**, 12967 (2021).
- [62] See Supplemental Material at <http://link.aps.org/supplemental/10.1103/PhysRevA.106.013509> for the video about the rotation process of particles related to Figs. 5(c1)–5(c5) when the circular Pearcey-like vortex beam propagates along the hyperbolic secant trajectory.
- [63] O. Jovanovic, Photophoresis–Light induced motion of particles suspended in gas, *J. Quant. Spectrosc. Radiat. Transfer* **110**, 889 (2009).